

Chlorine adsorption on the Cu(111) surface

K. Doll⁺ and N. M. Harrison*

CLRC, Daresbury Laboratory, Daresbury, Warrington, WA4 4AD, UK

** and Department of Chemistry, Imperial College, London, SW7 2AY, UK*

⁺ Electronic address: k.doll@dl.ac.uk

Abstract

We investigate the adsorption of chlorine on the Cu(111) surface with full potential all-electron density functional calculations. Chlorine adsorption at the fcc hollow sites is slightly preferred over that at the hcp hollow. The adsorption geometry is in excellent agreement with electron diffraction and ion scattering data. Adsorption energies and surface diffusion barriers are close to those deduced from experiment.

I. INTRODUCTION

The determination of surface structure and adsorption energetics is a key issue in surface science¹. Adsorption on metallic surfaces is of particular importance due to its relevance to many industrial processes. First principles simulation, based on density functional theory, is now one of the key tools for studying and developing an understanding of these systems².

The adsorption of halides on metal surfaces and especially Cl on Cu(111) has been the subject of extensive experimental studies. The first study in 1977 reported on results from low energy electron diffraction (LEED), Auger electron spectroscopy (AES), work function measurements and desorption experiments³. Further work has been performed using surface extended X-ray absorption fine structure (SEXAFS) and photoelectron diffraction^{4,5}, normal incident X-ray standing wavefield absorption (NIXSW)⁶⁻⁹, secondary ion mass spectrometry (SIMS)¹⁰, scanning tunneling microscopy (STM)¹¹, LEED, AES, thermal and electron stimulated desorption¹². However, we are not aware of any first principles simulations of this system. This is no doubt in part due to the large computational effort needed to study the complex surface geometry with sufficient accuracy. In this article we present the results of an extensive study of the surface adsorption geometry and energetics within a gradient-corrected density functional formalism. It turns out that a very high accuracy is necessary to distinguish the different adsorption sites and thus careful calculations capable of resolving energy differences of the order of only a few meV are required. In view of this we present details of the tests performed to establish the numerical accuracy of the calculations.

The outline of the article is as follows. In section II, we give the details of the computational method. In section III, we present results for bulk Cu which document the accuracy of the numerical methodology and the functional used. In section IV, the surface geometry and energetics of the clean Cu surface are presented. The important numerical approximation of reciprocal lattice sampling is discussed in detail. In section V we present a quantitative description of the adsorption of Cl on the (111) surface of Cu.

II. METHOD

The fundamental approximation made in density functional calculations is the choice of the effective one-particle potential. In this study we employed three distinct approximations: the local density approximation (LDA) with Dirac-Slater exchange¹³ and the Perdew-Zunger correlation functional¹⁴; the gradient corrected exchange and correlation functional of Perdew and Wang (GGA)¹⁵; and the Hartree-Fock (HF) approximation.

A local basis scheme based on atom-centred Gaussian type orbitals was used. The calculations were performed with the CRYSTAL98 software¹⁶. The Cu basis set was chosen as $[6s5p2d]$ ¹⁷. The values of the inner exponents (a set consisting of one s contraction, 3 sp contractions and 1 d contraction, i.e. $[4s3p1d]$), is given in table I. The outermost exponents were optimized in calculations on copper bulk at the GGA, LDA, and HF level. It is interesting to note that for Cu, in contrast to lithium¹⁸, it is possible to optimize the total energy with respect to the exponents without numerical difficulties even in the HF approximation. We believe that this is due to the more localized nature of the orbitals in Cu.

For Cl the $[5s4p]$ basis set developed in previous calculations on alkali halides was used¹⁹, with outermost sp exponents of 0.294 and 0.090. An additional d -function with exponent 0.5 was added yielding a $[5s4p1d]$ set.

The density functional potential was fitted with an auxiliary basis set, which consisted, for both Cu and Cl, of 12 s and p functions with exponents taken to be a geometrical sequence from 0.1 to 2000, and 5 d functions with exponents in the range 0.8 to 100.

As in a recent study of lithium²⁰, we employ finite temperature density functional theory²¹ to ease the numerical integration over \vec{k} -space with the occupation calculated according to the Fermi function at finite temperature T (Ref. 22) and the zero temperature energy is approximated by²³ $\frac{1}{2}(E(T) + F(T))$; with E the energy and F the free energy $F = E - TS$, where S is the electronic free entropy. The important approximation associated with the choice of the sampling nets employed in reciprocal space integration will be

discussed in detail below.

III. BULK PROPERTIES

We calculated the band structure and cohesive properties of Cu bulk in order to document the performance of our numerical approximations and to compare different choices for the effective one-particle potential (LDA, GGA, and HF).

Figure 1 displays the LDA band structure for bulk copper which is in excellent agreement with that reported in the literature²⁴. The LDA band structure remains virtually unchanged when only LDA exchange is included. Using GGA exchange and correlation leads to a similar band structure. The Hartree-Fock band structure (figure 2) reveals the expected pathology associated with the non-local exchange interaction and neglect of correlation in a metal. The overall bandwidth is too large by a factor of nearly two and the *d*-bands too low in energy compared to the wide *4sp* band.

The structure and cohesive properties are reported in table II. The GGA cohesive energy, lattice constant and bulk modulus are in good agreement with those observed. The LDA tends to over-bind the system resulting in a somewhat too low lattice constant and thus a high bulk modulus. The HF solution is dramatically underbound, the lattice constant far too large and thus the bulk modulus is very low. It is clear that the structure and energetics of the bulk crystal are best described within the GGA.

IV. CU SURFACES

We studied the clean Cu surface in some detail in order to establish the accuracy of predicted surface structures and energies.

We used two methods to compute the surface energy^{25,20}. Firstly, by extrapolating from calculations on slabs with a different number of layers (*n* and *m*):

$$E_{surface} = \frac{1}{2}(E_{slab}(n) - (E_{slab}(n) - E_{slab}(n - m))\frac{n}{m}) \quad (1)$$

and secondly by using an independent bulk energy:

$$E_{surface} = \frac{1}{2}(E_{slab}(n) - E_{bulk} \times n) \quad (2)$$

where all the quantities $E_{surface}$, $E_{slab}(n)$, and E_{bulk} are expressed as energies per atom. In Ref. 20, we gave a detailed comparison of the application of both formulas to the Li surface. The electronic structure of Cu is more complex than Li so as a first step we investigated the dependence of the surface energies on the electronic temperature and number of sampling points.

We focus the discussion now on the Cu (111) surface. In figure 3, we display the temperature and sampling point dependence of the surface energy obtained from equation 1 using two slabs with 3 and 4 layers. The density of reciprocal lattice points is determined by a shrinking factor. We used different shrinking factors of 2, 4, 8, 12, and 16 which result in 2, 4, 10, 19, and 30 points in the irreducible part of the Brillouin zone. As expected the surface energy converges with respect to \vec{k} -point sampling at higher temperatures but as the temperature is raised the extrapolation to the athermal limit becomes less accurate.

For the very high accuracy required in the current study we selected a shrinking factor of 16 and a temperature of $k_B T = 0.01 E_h$ ($E_h = 27.2114$ eV). This converges the total energy of the bulk to better than $0.1 mE_h$, and that of the three layer copper slab to better than $0.3 mE_h$. In table III, we show the variation of the computed surface energy with slab thickness obtained both with equation 1 and 2. The convergence of the data based on equation 2 demonstrates the independent convergence of the bulk and slab energies with respect to \vec{k} -space sampling. This is an important prerequisite for accurate studies of chemical processes at surfaces. In many surface studies bulk cells and \vec{k} -space sampling are chosen to eliminate systematic errors in the definition of the surface energy. We note that this is not sufficient to guarantee the accuracy of surface properties.

Table IV contains the computed surface energies of copper. As found in earlier studies on the homogeneous electron gas¹⁵ and lithium²⁰, the LDA calculation results in a higher surface energy than the GGA. Previous LDA results^{26,27} are rather scattered but in reasonable

agreement with those computed here.

In addition, we studied the relaxation of the Cu (111) surface. For this purpose, the top layer of various slabs of different thickness was allowed to relax with the layer spacing within the slab fixed at the bulk value of $\frac{3.63\text{\AA}}{\sqrt{3}}$. The results in table V demonstrate that convergence is achieved for slabs with 4 or more layers. The computed inwards relaxation of 1.0 % is in very good agreement with recent experiments using medium-energy ion scattering (MEIS)²⁸ where a contraction of $1.0\pm 0.4\%$ was measured for the first interlayer spacing; it also agrees with that deduced from LEED experiments where inwards relaxations of $0.3\pm 1\%$ ²⁹ and $0.7\pm 0.5\%$ ³⁰ have been reported. A previous LDA calculation reported a relaxation of -1.27% ²⁶. In this calculation the second interlayer spacing, which we kept fixed at the bulk value, was also reported to decrease by 0.64 % while an experimental study²⁸ found a decrease of 0.2 %. We find that the relaxation of the top layer reduces the surface energy very slightly (by $0.003 \frac{J}{m^2}$).

V. CHLORINE ADSORPTION ON THE CU(111) SURFACE

The adsorption of chlorine on the Cu(111) surface was first studied by Goddard and Lambert³. At a coverage of one third of a monolayer, a structure displaying long range order in a $\sqrt{3} \times \sqrt{3}$ R30° pattern was observed and a desorption energy of 236 kJ/mol was obtained (see also Ref. 12). More recently the $\sqrt{3} \times \sqrt{3}$ R30° pattern has been confirmed in STM images¹¹. The distance between the Cl layer and the surface Cu layer has also been deduced from SEXAFS and photoelectron diffraction experiments^{4,5}. In this study, a distance of 2.39 ± 0.02 Å between nearest Cl-Cu neighbours was obtained (corresponding to an interlayer spacing of 1.88 ± 0.03 Å); the adsorption site was identified as the fcc (face centered cubic) hollow (see figure 4)³¹. A distance of 1.81 ± 0.05 Å between the Cl layer and a notional Cu-layer corresponding to unrelaxed bulk termination was deduced from NIXSW data⁶⁻⁸. Comparing the latter two results (SEXAFS and NIXSW) gives evidence for a slight inwards relaxation of the surface Cu layer similar to that observed on the clean

surface. SIMS measurements¹⁰ yield an interlayer spacing of $1.87 \pm 0.04 \text{ \AA}$. Recently, in NIXSW measurements, the fcc site was confirmed as the adsorption site, but also a small occupation of the hcp (hexagonal closed packed) hollow was observed⁹.

We optimized the structure of a slab with a chlorine coverage of one third of a monolayer in a $\sqrt{3} \times \sqrt{3}$ R30° cell. GGA calculations with the computational parameters described in section IV were performed which led to 73 sampling points in the irreducible part of the reciprocal lattice. Slabs consisting of 3 and 4 layers of Cu were used in which the Cu atoms in the top layer and the Cl layer were allowed to relax perpendicular to the surface. Cl was adsorbed in a number of sites; the threefold hcp hollow, the threefold fcc hollow, a top position, and a bridge position (figure 4).

The relaxed geometries and adsorption energies are presented in table VI. Adsorption on the fcc or hcp sites is clearly preferred over adsorption on bridge or top sites (by 3 and 17 mE_h , respectively). The Cl-Cu interlayer distance is 1.89 \AA for the fcc hollow (1.90 \AA for the hcp hollow) in excellent agreement with that deduced from experiment. The next neighbour Cl-Cu distance is 2.40 \AA for the fcc site, 2.41 \AA for the hcp site, 2.33 \AA for the bridge site and 2.17 \AA for the top site. This is consistent with the idea that the next-neighbour bond strength is greater, and therefore the bond shorter, when fewer nearest neighbours are available³². The inwards relaxation of the copper layer of $\sim 0.04 \text{ \AA}$ (1.9 %) is insensitive to the Cl adsorption site and similar to that found for the clean surface (1.7 %, table V).

The energy difference between the fcc and hcp sites is 0.3 mE_h and increases to 0.4 mE_h when the Cu surface is relaxed. To investigate the dependence of this rather delicate result on the number of layers of the slab, we performed similar calculations for fcc and hcp site on a four layer slab. The fcc site remains the preferred one by 0.2 mE_h . The relaxed surface geometry (i.e. the interlayer distance Cl-Cu) is identical to that computed for the three layer slab. The relaxation of the top Cu layer reduces slightly to 0.03 \AA (1.4 %) which is a similar trend as for the clean surface (table V). This value is within the errorbars of

the experimentally expected value. The optimization indicates that the fcc site is becoming more stable relative to the hcp site as the interlayer spacing between Cl and the second Cu layer is reduced. This is demonstrated in Figure 5 where, at a fixed interlayer spacing of 1.886 Å between Cl and the top Cu layer, the top Cu layer is allowed to relax inwards. As the relaxation increases, the fcc site becomes more stable with respect to the hcp site. The small energy difference between the fcc and hcp adsorption sites is in agreement with observations of predominantly fcc-site adsorption accompanied by a small occupancy of the hcp site⁹.

The calculated adsorption energy of $0.135 E_h$ (per Cl atom) is in reasonable agreement with that deduced from desorption measurements (~ 250 kJ/mol corresponding to $0.095 E_h$)^{3,12}. The experimental desorption energy is obtained from an Arrhenius model and therefore depends on a pre-exponential factor which was chosen to be $10^{13} \frac{1}{s}$ (Ref. 3,12), but questioned in Ref. 3.

The activation energy for surface diffusion was measured experimentally by electron stimulated diffusion¹², i.e. the activation energy for Cl atoms to diffuse into an area where Cl depletion is induced by an electron beam. A value of 19 kJ/mol or $7 mE_h$ was measured. A crude estimate from our calculations is possible if we assume that the energy difference of $3 mE_h$ between the hollow site and the bridge site is of the order of the activation energy for diffusion.

VI. CONCLUSION

We have demonstrated that a quantitative description of the adsorption of Cl on the Cu(111) surface can be achieved with full potential, all-electron, GGA calculations. The surface structure and adsorption energies are in excellent agreement with experiment. The Cl-Cu bond length is found to be 1.89 Å and the top Cu layer relaxes inwards by 1.4 %. The fcc hollow is found to be the preferred adsorption site, with the hcp site being $\sim 0.2 mE_h$ (5 meV) higher in energy. The energy difference between the two sites is sufficiently small

that it may alter slightly if a larger slab geometry was considered. Similarly, by analogy to the results for the clean Cu slab we might expect the inwards relaxation of 1.4 % to become slightly lower with larger slab geometries. The adsorption energy and surface diffusion energy is in reasonable agreement with those which can be estimated from experiment. Bulk and surface properties of Cu metal are found to be in very good agreement with experiment and previous calculations, when the gradient corrected GGA functional is used.

VII. ACKNOWLEDGMENTS

The authors would like to acknowledge support from EPSRC grant GR/K90661.

REFERENCES

- ¹ A. Zangwill, *Physics at Surfaces*, University Press, Cambridge (1988).
- ² M. Scheffler and C. Stampfl in: *Handbook of Surface Science*, Vol. 2: *Electronic Structure*, Editors: K. Horn and M. Scheffler, Amsterdam (1999).
- ³ P. J. Goddard and R. M. Lambert, *Surf. Science* **67**, 180 (1977).
- ⁴ M. D. Crapper, C. E. Riley, P. J. J. Sweeney, C. F. McConville, and D. P. Woodruff, *Europhys. Lett.* **2**, 857 (1986).
- ⁵ M. D. Crapper, C. E. Riley, P. J. J. Sweeney, C. F. McConville, D. P. Woodruff, *Surf. Science* **182**, 213 (1987).
- ⁶ D. P. Woodruff, D. L. Seymour, C. F. McConville, C. E. Riley, M. D. Crapper, N. P. Prince, R. G. Jones, *Phys. Rev. Lett.* **58**, 1460 (1987).
- ⁷ D. P. Woodruff, D. L. Seymour, C. F. McConville, C. E. Riley, M. D. Crapper, N. P. Prince, R. G. Jones, *Surf. Science* **195**, 237 (1988).
- ⁸ J. Lüdecke, S. Skorda, G. J. Jackson, D. P. Woodruff, R. G. Jones, B. C. C. Cowie, R. Ithnin, and C. A. Papageorgopoulos, *J. Phys.: Condensed Matter* **9**, 4593 (1997).
- ⁹ M. F. Kadodwala, A. A. Davis, G. Scragg, B. C. C. Cowie, M. Kerkar, D. P. Woodruff, R. G. Jones, *Surf. Science* **324**, 122 (1995).
- ¹⁰ W. K. Way, A. C. Pike, S. W. Rosencrance, R. M. Braun, and N. Winograd, *Surface and Interface Analysis* **24**, 137 (1996).
- ¹¹ K. Motai, T. Hashizume, H. Lu, D. Jeon, T. Sakurai, and H. W. Pickering, *Applied Surface Science* **67**, 246 (1993).
- ¹² W. K. Walter, D. E. Manolopoulos, R. G. Jones, *Surf. Science* **348**, 115 (1996).
- ¹³ P. A. M. Dirac, *Proc. Camb. Phil. Soc.* **26**, 376 (1930); J. C. Slater, *Phys. Rev.* **81**, 385

- (1951);
- ¹⁴ J. P. Perdew and A. Zunger, *Phys. Rev. B* **23**, 5048 (1981).
- ¹⁵ J. P. Perdew, J. A. Chevary, S. H. Vosko, K. A. Jackson, M. R. Pederson, D. J. Singh, and C. Fiolhais, *Phys. Rev. B* **46**, 6671 (1992).
- ¹⁶ V. R. Saunders, R. Dovesi, C. Roetti, M. Causà, N. M. Harrison, R. Orlando, C. M. Zicovich-Wilson *CRYSTAL 98 User's Manual*, Theoretical Chemistry Group, University of Torino (1998).
- ¹⁷ M. D. Towler, R. Dovesi, and V. R. Saunders, *Phys. Rev. B* **52**, 10150 (1995).
- ¹⁸ R. Dovesi, E. Ferrero, C. Pisani, and C. Roetti, *Z. Phys. B* **51**, 195 (1983).
- ¹⁹ M. Prencipe, A. Zupan, R. Dovesi, E. Aprà, and V. R. Saunders, *Phys. Rev. B* **51**, 3391 (1995).
- ²⁰ K. Doll, N. M. Harrison, and V. R. Saunders, *J. Phys.: Condensed Matter* **11**, 5007 (1999).
- ²¹ N. D. Mermin, *Phys. Rev.* **137**, A 1441 (1963).
- ²² C. L. Fu and K. M. Ho, *Phys. Rev. B* **28**, 5480 (1983).
- ²³ M. J. Gillan, *J. Phys. C* **1**, 689 (1989).
- ²⁴ There are numerous publications on the Cu band structure, and we give only one example: O. Jepsen, D. Glötzel, and A. R. Mackintosh, *Phys. Rev. B* **23**, 2684 (1981) (and references therein).
- ²⁵ J. C. Boettger and S. B. Trickey, *Phys. Rev. B* **45**, 1363 (1992); J. C. Boettger, *Phys. Rev. B* **49**, 16798 (1994).
- ²⁶ Th. Rodach, K.-P. Bohnen, and K. M. Hu, *Surf. Science* **286**, 66 (1993).
- ²⁷ H. L. Skriver and N. M. Rosengaard, *Phys. Rev. B* **46**, 7157 (1992).

- ²⁸ K. H. Chae, H. C. Lu, and T. Gustafsson, Phys. Rev. B **54**, 14082 (1996).
- ²⁹ S. P. Tear, K. Röhl, and M. Prutton, J. Phys. C: Solid State Phys. **14**, 3297 (1981).
- ³⁰ S. Å. Lindgren, L. Walldén, J. Rundgren, and P. Westrin, Phys. Rev. B **29**, 576 (1984).
- ³¹ Graphics generated with DL Visualize, <http://www.cse.clrc.ac.uk/Activity/DLV>
- ³² L. Pauling, The nature of the chemical bond and the structure of molecules and crystals, Cornell University Press (1960).
- ³³ J. F. Janak, V. L. Moruzzi, and A. R. Williams, Phys. Rev. B **12**, 1257 (1975).
- ³⁴ C. M. Fehrenbach and H. Bross, Phys. Rev. B **48**, 17703 (1993) and references therein.
- ³⁵ K. A. Gschneidner, Jr., Solid State Phys. **16**, 276 (1964).
- ³⁶ W. C. Overton and J. Gaffney, Phys. Rev. **98**, 969 (1955).

TABLES

TABLE I. The $[6s5p2d]$ copper basis set with the two outermost sp exponents and the outermost d exponent optimized within the GGA. Those based on LDA and HF are shown in brackets.

	exponent	s contraction	p contraction	d contraction
s	398000.0	0.000227		
	56670.0	0.001929		
	12010.0	0.01114		
	3139.0	0.05013		
	947.2	0.17031		
	327.68	0.3693		
	128.39	0.4030		
	53.63	0.1437		
sp	1022.0	-0.00487	0.00850	
	238.9	-0.0674	0.06063	
	80.00	-0.1242	0.2118	
	31.86	0.2466	0.3907	
	13.33	0.672	0.3964	
	4.442	0.289	0.261	
sp	54.7	0.0119	-0.0288	
	23.26	-0.146	-0.0741	
	9.92	-0.750	0.182	
	4.013	1.031	1.280	
sp	1.582	1.0	1.0	

<i>sp</i>	0.596 (LDA: 0.610; HF: 0.555)	1.0	1.0
<i>sp</i>	0.150 (LDA: 0.150; HF: 0.170)	1.0	1.0
<i>d</i>	48.54		0.031
	13.55		0.162
	4.52		0.378
	1.47		0.459
<i>d</i>	0.392 (LDA: 0.392; HF: 0.423)		1.0

TABLE II. The ground state properties of bulk copper. Energies are in Hartree units, lattice constants in Å, bulk moduli in GPa.

	a	E_{coh}	B
LDA	3.53	0.182	195
GGA	3.63	0.143	155
HF	3.95	0.018	69
Lit. (KKR) ³³	3.59	0.155	158
Lit. (LDA) ²⁶	3.62	0.133	147
exp.	3.604 ³⁴	0.129 ³⁵	142 ³⁶

TABLE III. The convergence of the surface energy of the Cu(111) surface as a function of the number of layers, computed using a shrinking factor of 16 and a smearing temperature of $0.01 E_h$. For the Cu(111) surface, $1 \frac{E_h}{atom}$ corresponds to $76.4 \frac{J}{m^2}$ for a lattice constant of 3.63 \AA .

number of layers	$E_{slab}(n)$	$E_{slab}(n) - E_{slab}(n-1)$	$E_{surface}$ using $E_{slab}(n) - E_{slab}(n-1)$	$E_{surface}$ using $E_{bulk} = -1640.698861$
	E_h	$\frac{E_h}{atom}$	$\frac{E_h}{atom}$	$\frac{E_h}{atom}$
1	-1640.653606	-	-	0.02263
2	-3281.350305	-1640.69670	0.02155	0.02371
3	-4922.049528	-1640.69922	0.02407	0.02353
4	-6562.748468	-1640.69894	0.02365	0.02349
5	-8203.447228	-1640.69876	0.02329	0.02354
6	-9844.146061	-1640.69883	0.02347	0.02355
7	-11484.844913	-1640.69885	0.02352	0.02356
8	-13125.543718	-1640.69881	0.02336	0.02359
9	-14766.242595	-1640.69888	0.02365	0.02358
10	-16406.941437	-1640.69884	0.02349	0.02359
11	-18047.640289	-1640.69885	0.02354	0.02359

TABLE IV. The surface energy ($\frac{J}{m^2}$) of the low index copper surfaces.

surface	LDA	GGA	Ref. 27 (LDA) ; Ref. 26 (LDA)
(100)	2.52	2.01	2.09 ; 1.712
(110)	2.67	2.15	2.31 ; 1.846
(111)	2.26	1.80	1.96 ; 1.585

TABLE V. Relaxation of Cu (111) surface, as a function of the number of layers, computed within the GGA. The top layer is allowed to relax, the other layers are kept at a fixed distance of $\frac{3.63\text{\AA}}{\sqrt{3}}$ corresponding to the bulk lattice constant

number of layers	relaxation in Å (in %)
3	-0.035 (-1.7 %)
4	-0.025 (-1.2 %)
5	-0.023 (-1.1 %)
6	-0.022 (-1.0 %)
Literature:	
exp. ²⁸	-1.0 ± 0.4 %
exp. ²⁹	-0.3 ± 1 %
exp. ³⁰	-0.7 ± 0.5 %
LDA ²⁶	-1.27 %

TABLE VI. Adsorption of Cl on the Cu(111) surface. δ_{1-2} is the change in interlayer spacing between first and second copper layers (in Å) relative to the bulk value, $d_{\text{Cl-Cu top layer}}$ is the distance between the Cl and top Cu layer (in Å). The adsorption energy is the difference $E_{\text{Cl at Cu(111)}} - E_{\text{Cu(111)}} - E_{\text{Cl}}$.

n	δ_{1-2}	$d_{\text{Cl-Cu top layer}}$	$E_{\text{adsorption}}$ in E_h , per Cl atom
fcc site			
3	0 (no relaxation allowed)	1.89	0.13542
3	-0.043	1.89	0.13566
4	-0.032	1.89	0.13583
hcp site			
3	0 (no relaxation allowed)	1.90	0.13510
3	-0.038	1.90	0.13527
4	-0.031	1.90	0.13563
bridge site			
3	-0.040	1.94	0.13265
top site			
3	-0.041	2.17	0.11888

FIGURES

FIG. 1. LDA band structure at the equilibrium lattice constant.

FIG. 2. HF band structure at the equilibrium lattice constant.

FIG. 3. (111) Copper surface energy with four different reciprocal lattice samplings extracted from two slabs with 3 and 4 layers using $\frac{1}{2}(E(T) + F(T))$ and equation 1

FIG. 4. The structures considered for Cl, adsorbed on the Cu(111) surface at one third coverage, in a $\sqrt{3} \times \sqrt{3}$ R30° unit cell. When Cl is adsorbed in an fcc hollow, it sits above a Cu atom in the third layer (upper left) while in the hcp hollow it is above an atom in the second layer (upper right). The top position is Cl adsorbed vertically above a surface atom (lower left). In the bridge position it is vertically above the middle of two surface atoms (lower right).

FIG. 5. Total energy and energy difference of fcc and hcp adsorption site as a function of the inwards relaxation of the top Cu layer. The data in this figure is from a four-layer slab at a fixed interlayer spacing between Cl and top Cu layer of 1.886 Å for both fcc and hcp adsorption site.

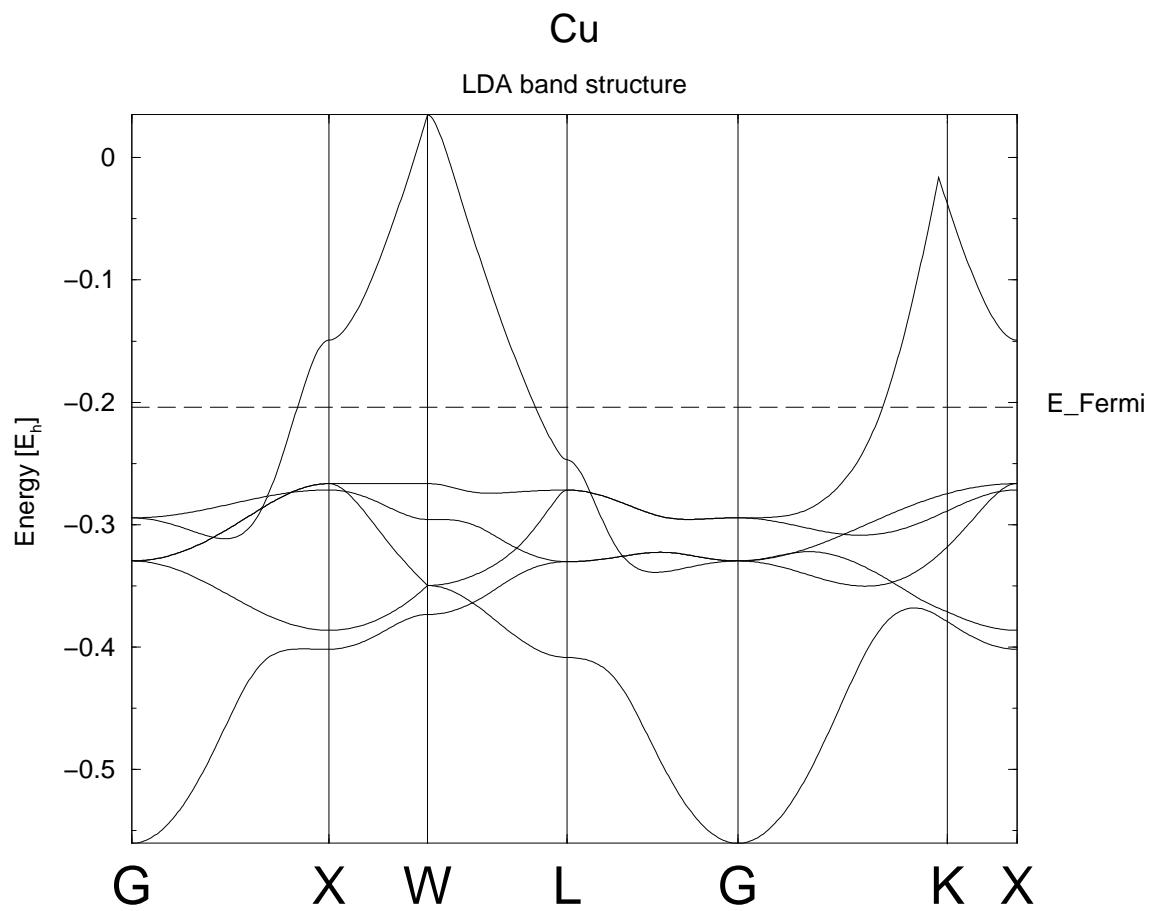


Fig. 1

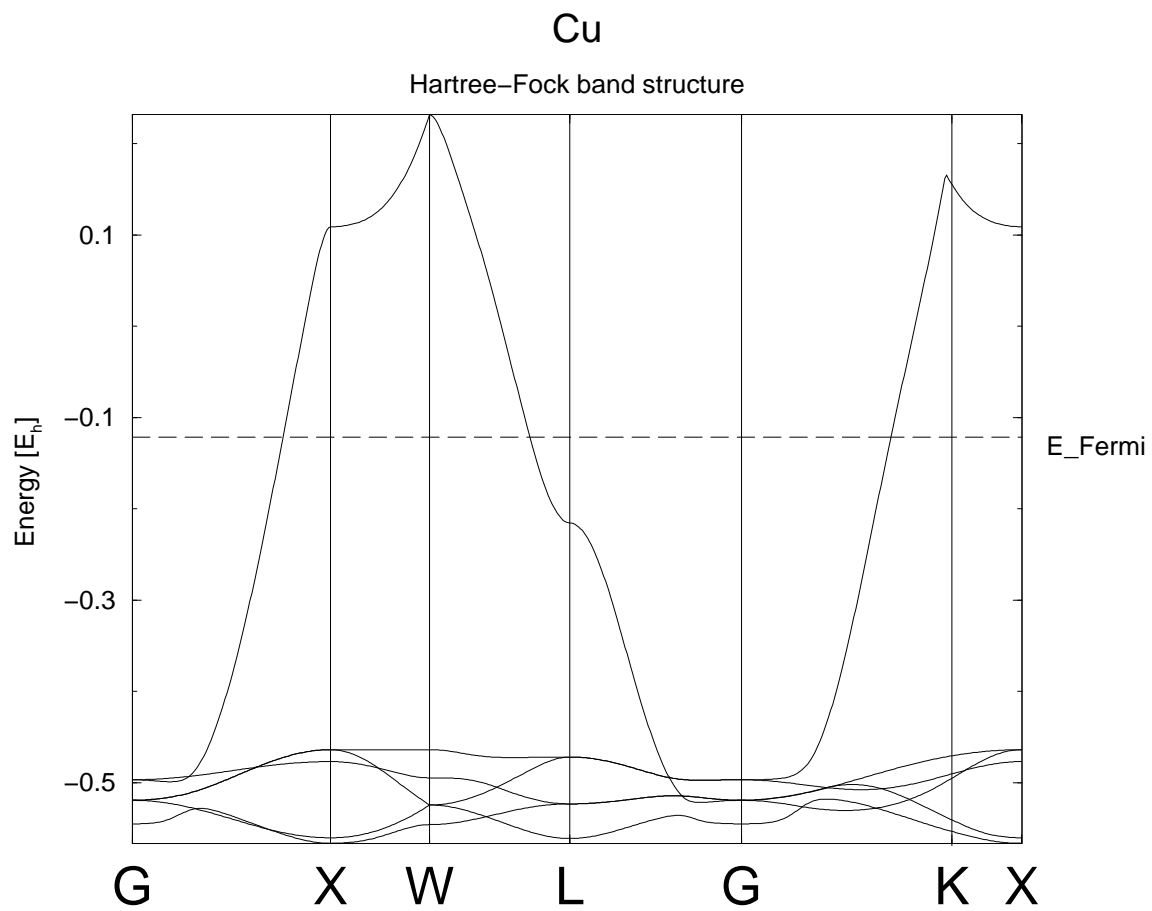


Fig. 2

Cu (111) surface

GGA

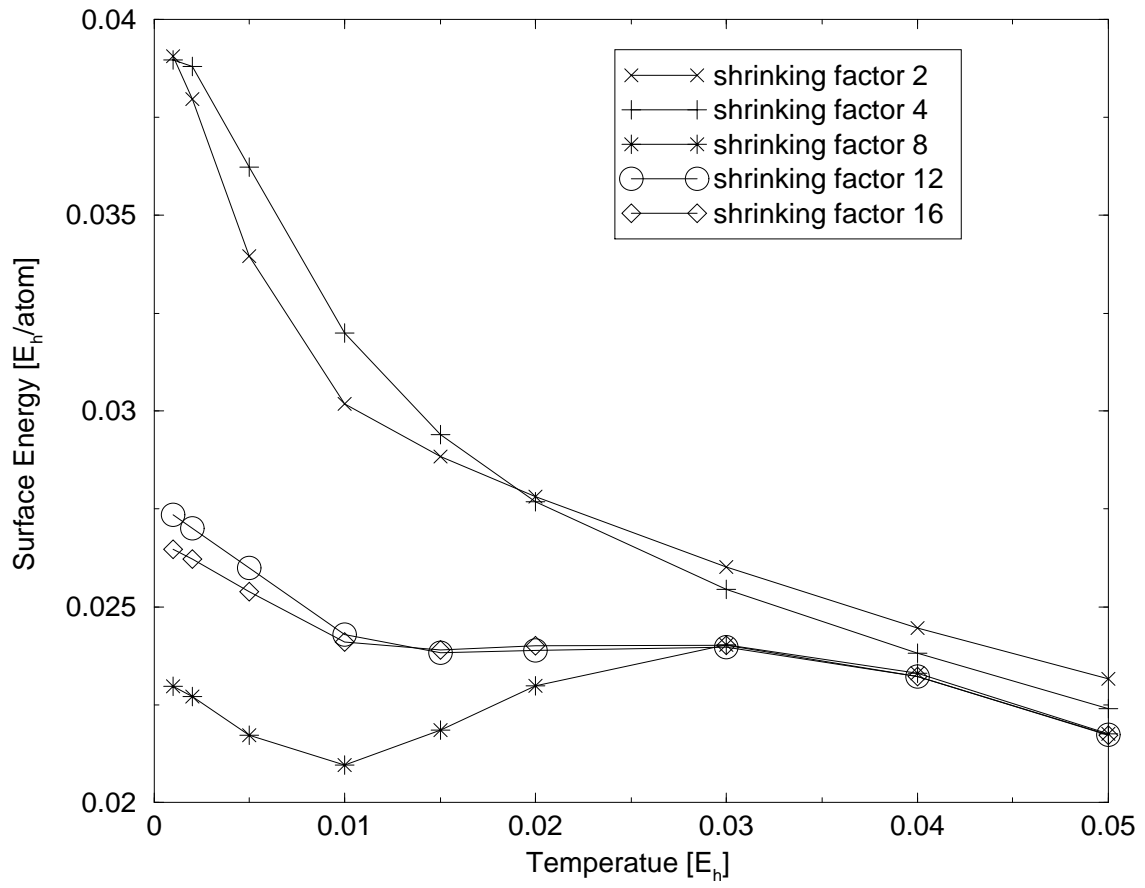
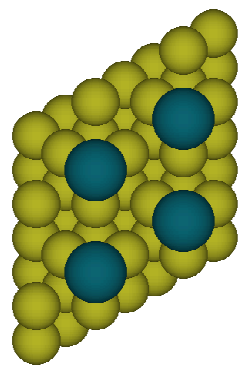
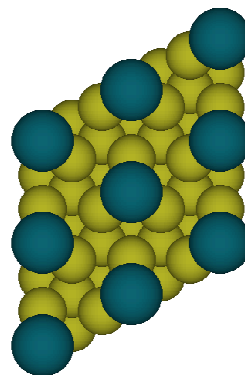


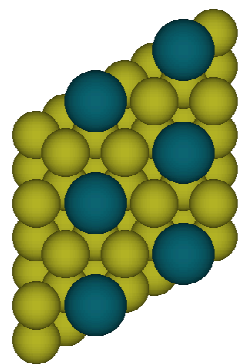
Fig. 3



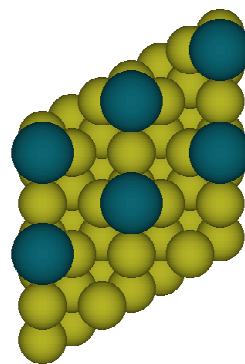
fcc



hcp



top



bridge

Fig. 4

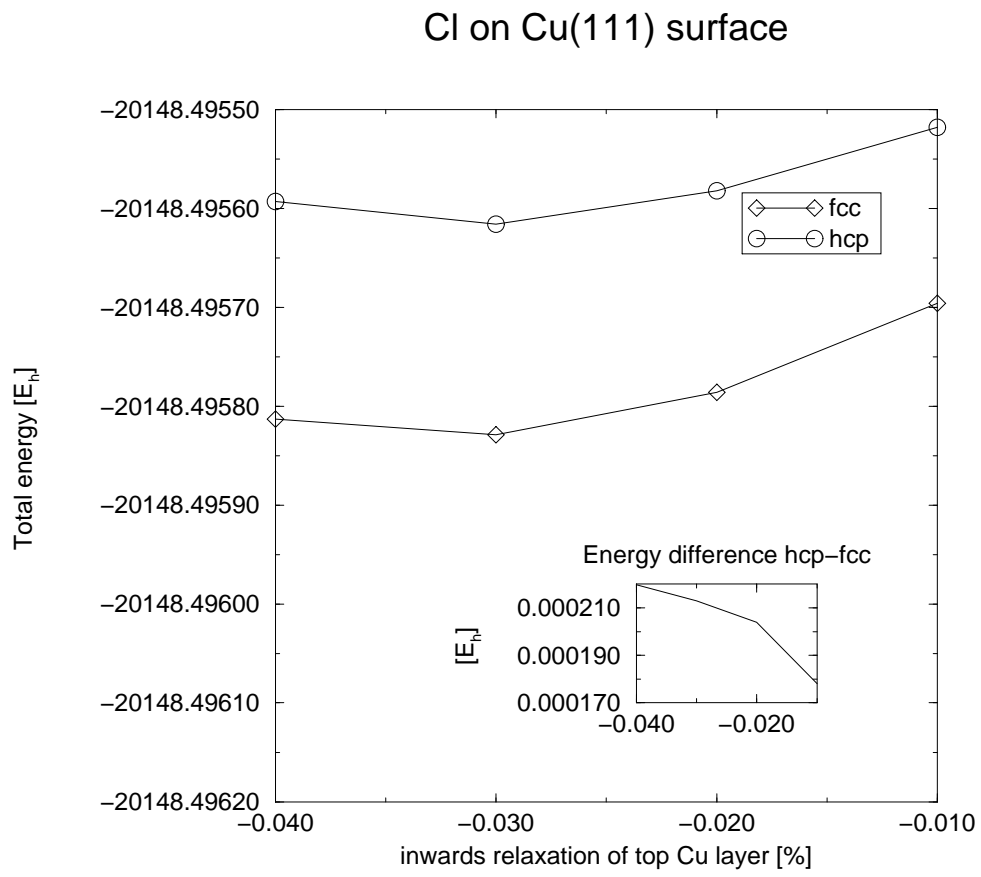


Fig. 5